Research paper

Effect of a small dike on blast wave propagation

Yuta Sugiyama*†, Kunihiko Wakabayashi*, Tomoharu Matsumura*, and Yoshio Nakayama*

*National Institute of Advanced Industrial Science and Technology (AIST),
Central 5, 1−1−1 Higashi, Tsukuba, Ibaraki 305−8565, JAPAN
Phone : +81−29−861−0552
†Corresponding author : yuta.sugiyama@aist.go.jp

Received : January 6, 2015 Accepted : March 31, 2015

Abstract

This paper, by means of numerical simulations and experiments, investigates the effect of a small dike on the propagation of a blast wave so as to extract factors related to the strength of the blast wave on the ground. Three materials were considered in this study : detonation products, steel, and air. A cylindrical charge of pentaerythritol tetranitrate (PETN), with a diameter to height ratio of 1.0, was used in the experiments and numerical simulations. A steel dike surrounded the explosive charge on all sides. Its shape and size were parameters in this study. To elucidate the effect of the dike, we conducted two series of numerical simulations and experiments : one without a dike and one with a dike. Peak overpressures on the ground agreed with the experimental results. The numerical simulations qualitatively showed the effect of the three-dimensional diffraction and reflection of the blast wave at the dike, which affected the propagation behavior of the blast wave.

Keywords : numerical simulation, experiment, blast wave, dike effect, directional characteristics

1. Introduction

High-energetic materials yield powerful energy instantly, and are used widely in industrial technologies. However, an accidental explosion of high explosives creates a blast wave and fragments, which are a hazard to people and have the potential to cause extensive damage to property. Various means of minimizing the effects of such an explosion have long been investigated. A dike and wall are often used to weaken the blast wave on the ground and to hold the fragments caused by the explosion[1)−6)]. When a dike is located near the center of an explosion, the blast wave reflects and diffracts at the dike. The disturbed blast wave gives rise to peak overpressures with directional characteristics on the ground. Therefore, for the practical use of a dike, effects such as the diffraction and reflection of the blast wave have been specified in laws governing the control of explosives. The AIST has been conducting small-scale explosion experiments to be able to discuss blast wave strength with newly designed dikes constructed of soil and steel, but the effect of a dike has not been understood well by experiments alone. As numerical simulations can provide large quantities of data, they serve as good alternatives to explosion experiments having complex physics with the interaction of the blast wave and a dike. We have been formulating our own numerical program, and in an early study validated a multicomponent flow method for modeling a blast wave problem attenuated by a water wall[7),8)] and a steel wall[6)]. In this paper, we conducted small-scale experiments and numerical simulations to understand explosion phenomenon with two types of dikes. The details of the experiments and numerical simulation are described in Sections 2 and 3. In Section 4, we validate our numerical data by comparing the data with the experimental results, and our numerical data reveal the propagation behavior of a blast wave disturbed by a dike. Our study qualitatively focuses on the effect of the reflection, diffraction, and three-dimensional structure, separately.

2. Experimental setup

Figure 1 shows the experimental setup, which consists of a pellet of high explosive, an ignitor, and pressure transducers for a 45°-dike at y = 0. The pressed pellet consists of 95 weight % of pentaerythritol tetranitrate (PETN) and 5 weight % of carbon powder. The pellet is cylindrical with a diameter and length of 7.5 mm. The weight and density of the pellet are 0.5 g and 1509 kg m^{-3},

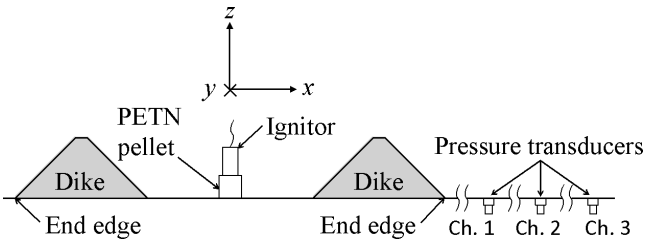

Figure 1 Setup of a pellet of PETN high explosive, ignitor, and pressure transducers for a 45° -dike at $y = 0$.

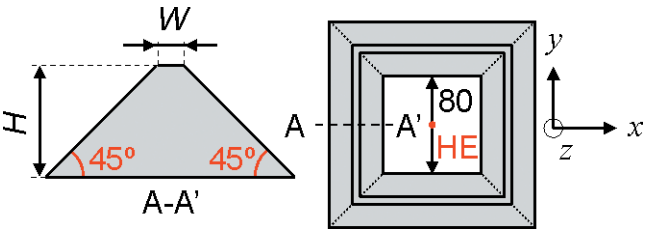

(a) 45° -dike

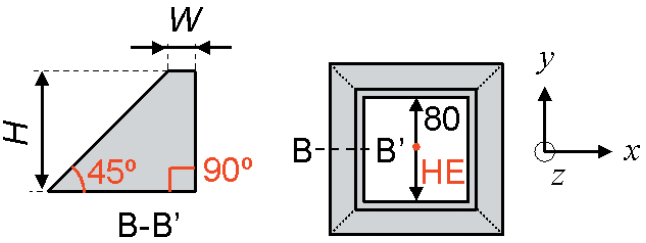

(b) 90° -dike

Figure 2 Details of dikes with height H and width W on the ground ($z = 0$)

respectively. A specially designed electric detonator, whose main primary explosive is 100 mg of lead azide, is used as shown in Figure 1. The supplier of the explosives and detonators is Showa Kinzoku Kogyo Co., Ltd. The detonator is glued to the top of the pellet, which is then placed on the ground. Three pressure transducers are used to measure the blast pressure, and their distances (scaled distance by weight of high explosive) are 340 mm (4.3 m kg$^{-1/3}$), 740 mm (9.3 m kg$^{-1/3}$), and 1140 mm (14.4 m kg$^{-1/3}$). Peak overpressures on the line of $y = 0$ at $z = 0$ are obtained in order to validate the numerical data. The dike is constructed of JIS SS400 steel. Figure 2 shows details of dikes with height H and width W. In this study, we investigate two types of dikes to show the effect of the slope of the dike. Cross section A-A' shows that the 45° -dike has 45° slopes on both sides, whereas B-B' shows that the 90° -dike has a 90° wall on the high explosive side and a 45-degree slope on the other side. The area inside the dike is constant at 80 mm square in all experiments. We change the size of dikes as shown in Table 1 and discuss the effect of height. Experiments without the dike are also conducted in order to investigate the mitigation and intensification of the blast wave by the dike. The experimental results show that the dispersion of the peak overpressures is less than 10%.

3. Numerical setup

We developed a multicomponent method[6)–8)] for three materials based on the five-equation model proposed by Allaire *et al*.[9)] In this study, we use three materials to reproduce the experiment. The ideal gas, stiffened gas, and Jones-Wilkins-Lee (JWL) equations of state are used to model air, steel, and the detonation products of PETN. The governing equations and parameters in the equations of state are fully described in our previous paper[6)]. Harten-Lax-Leer type (HLL) schemes are utilized to model contact surfaces and maintain accuracy with strong shock waves. We use the HLL/HLLC (HLL for Contact) scheme[10)–12)] for spatial integration, and conduct third-order MUSCL (Monotonic Upstream-centered Schemes for Conservation Laws) interpolation with a linear scaling limiter[13)]. The switching of the HLL and HLLC schemes is determined by the pressure ratio between a grid point and the other points around it. When the pressure ratio is larger than 2, the HLL scheme is used. The third-stage TVD Runge-Kutta method[14)] is used for time integration. Figure 3 shows the initial, grid, and boundary conditions for a 45° -dike. Grid points are shown in every 20 points. The finest and constant grid spacing of 1 mm is set at 0 mm $\le x \le$ 350 mm, 0 mm $\le y \le$ 350 mm, and 0 mm $\le z \le$ 200 mm. In other regions, the grid spacing gradually increases. To show the directional characteristics of the blast wave on the ground ($z = 0$ mm), the coarsest grid spacing is limited to 4 mm in the x and y directions at 350 mm $\le x$, and 350 mm $\le y$. A mirror condition (green) at $x = 0$ mm and $y = 0$ mm, a slip wall condition (blue) at $z = 0$ mm, and the outflow condition (not shown in Figure 3) at other boundaries are employed. The enlarged view shows a 45° -dike and the high-pressure detonation product of cylindrical PETN. After the calculation starts, the blast wave expands with reflection and diffraction at the dike, which causes the propagation of a disturbed blast wave.

Table 1 Dike shape parameters.

Dike shape	Height H [mm]	Width W [mm]
45° -dike	20	5
	40	
90° -dike	20	7
	40	

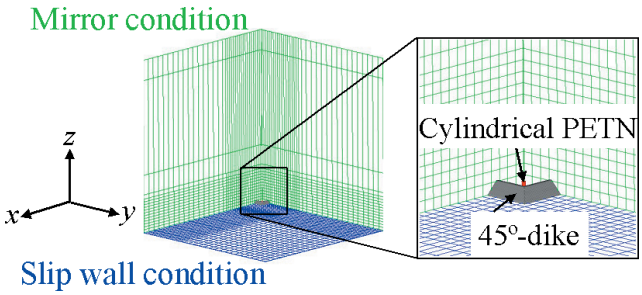

Figure 3 Initial, grid and boundary conditions for a 45° -dike. Grid points are shown in every 20 points.

4. Results

For safety analysis, we focus on peak overpressures and propagation of the blast wave on the ground. To discuss blast wave strength, peak overpressures of the experiments on the ground are used to validate those of the numerical results. Our data incorporate a scaled distance K, m kg$^{-1/3}$. A scaled distance of 1 m kg$^{-1/3}$ corresponds to 79.37 mm in this study. Figure 4 shows the numerical and experimental data of the peak overpressure on the ground at $y = 0$ for cases without a dike, with a 45°-dike, and with a 90°-dike. The height of dike H is 20 mm and 40 mm in Figures 4(a) and 4(b), respectively. The horizontal axis indicates the scaled distance, m kg$^{-1/3}$, in the x direction. Figure 5 shows the normalized peak overpressure distributions, and the horizontal axis indicates the scaled distance in the x direction. Here, peak overpressure distributions are normalized with respect to those in the case without a dike. Dashed line denotes the unity of the normalized peak overpressure. Therefore, it can be seen that the dike intensifies the blast wave when the normalized peak overpressure is larger than 1, whereas, the dike mitigates the blast wave when it is smaller than 1. In Figures 4 and 5, the plots and solid lines denote the experimental and numerical data, respectively. As the numerical lines agree with the experimental plots, our numerical method gives the correct estimation for the strength of the blast wave.

Peak overpressure decreases as the blast wave expands. As shown in Figures 4 and 5, the blast wave

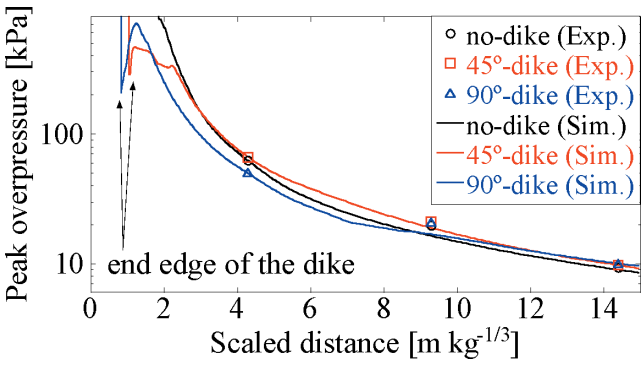

(a) Height $H = 20$ mm

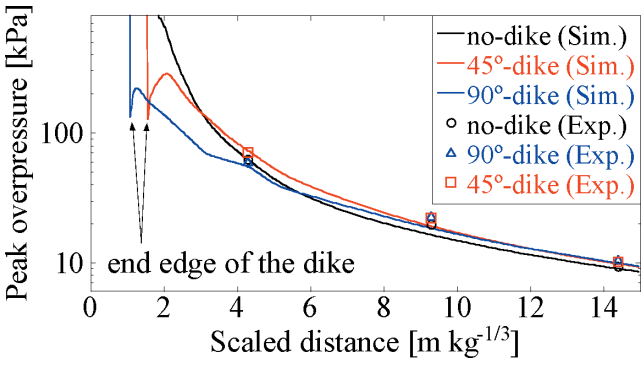

(b) Height $H = 40$ mm

Figure 4 Numerical and experimental data of the peak overpressure on the ground at $y = 0$ without a dike, with a 45°-dike, and with a 90°-dike.
Sim : Numerical simulations
Exp : Experiments

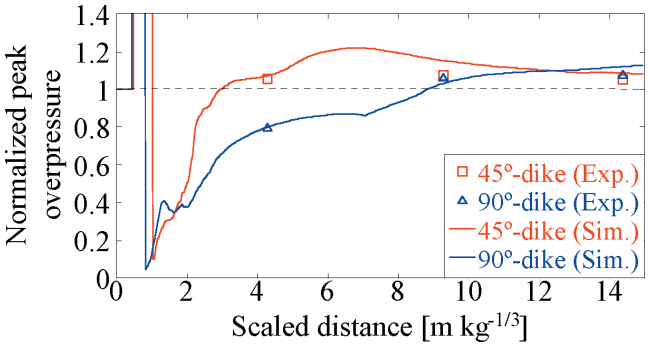

(a) Height $H = 20$ mm

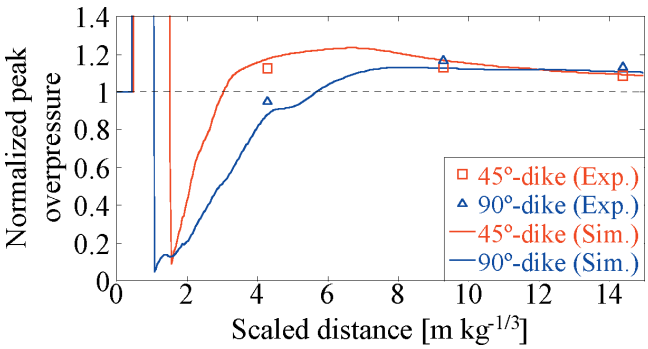

(b) Height $H = 40$ mm

Figure 5 Numerical and experimental data of the normalized peak overpressure distribution on the ground at $y = 0$ for a 45°-dike and for a 90°-dike. Peak overpressure distributions are normalized with respect to those without a dike. Dashed line denotes the unity of the normalized peak overpressure.
Sim : Numerical simulations
Exp : Experiments

around the end edge (the scaled distance around 1 m kg$^{-1/3}$) of the dike is well mitigated and the peak overpressures are around 10 % for a 45°-dike, and 5 % for a 90°-dike and without a dike. Therefore, the 90°-dike has a far greater mitigation effect near the dike. After the blast wave descends the dike and reflects off the ground near the end edge, the peak overpressures are locally intensified, and a disturbed blast wave with a triple point appears, as in the numerical data in Ref. 6. During the development of the disturbed blast wave, the normalized blast wave strength increases as it propagates. Far from the explosion point, numerical lines with dikes (blue and red) in Figure 4 show the same peak overpressure. Dikes intensify the blast wave on the ground at a large-scaled distance along $y = 0$, and the normalized peak overpressures converge to 110 % of that when there is no dike. The two types of dikes in this study do not show an advantage for the blast wave strength along $y = 0$ far from the explosion point.

Figure 6 shows the normalized peak overpressure distributions $p_{dike}/p_{no-dike}$ on the ground for (a) a 45°-dike with $H = 20$ mm, (b) a 90°-dike with $H = 20$ mm, (c) a 45°-dike with $H = 40$ mm, and (d) a 90°-dike with $H = 40$ mm. Black lines show that the normalized peak overpressures is 1. The 45°-dike gives the directional characteristics and has the potential to reduce the blast wave strength around the line of $y = x$ by the effect of the three-dimensional

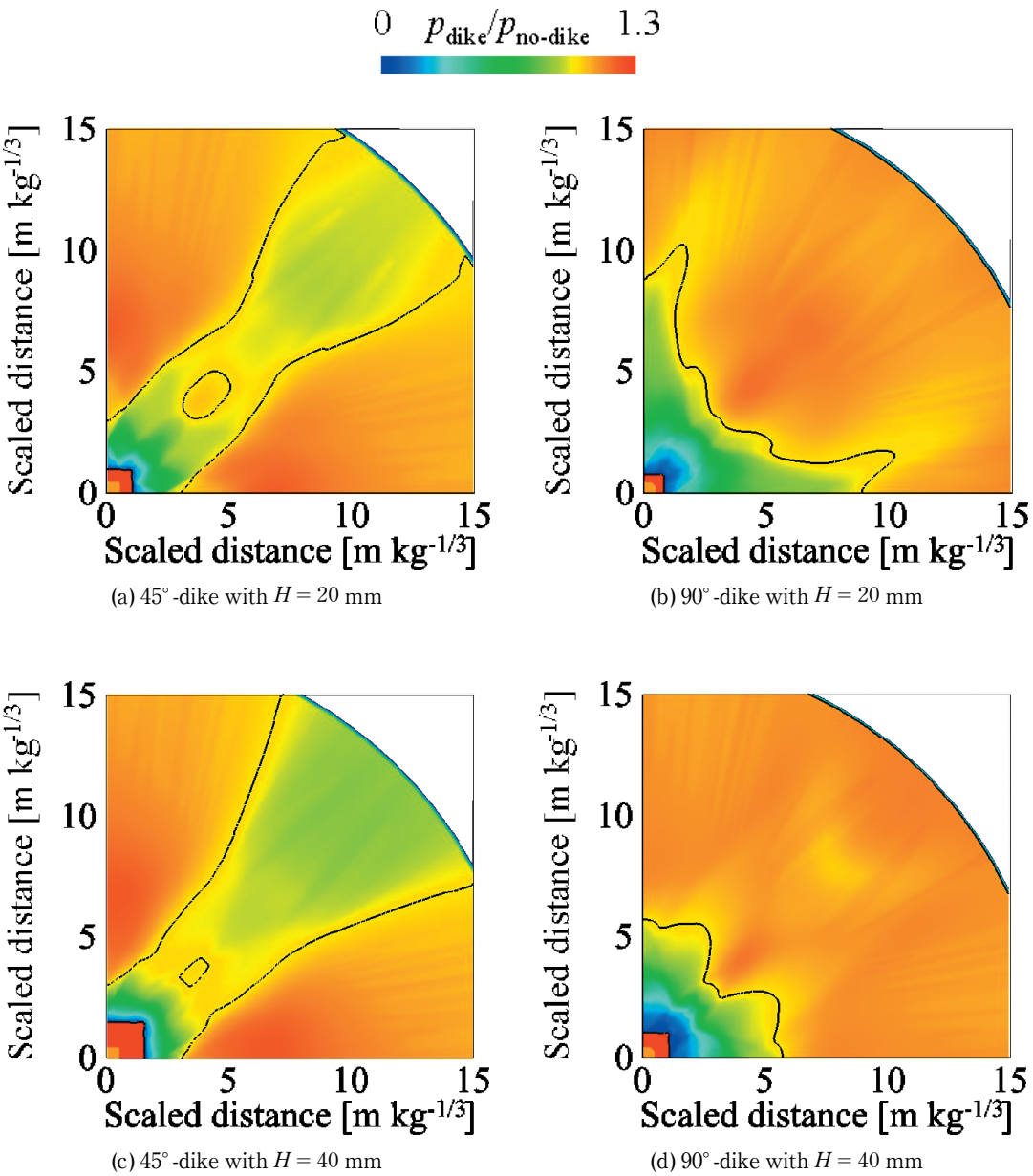

(a) 45° -dike with $H = 20$ mm

(b) 90° -dike with $H = 20$ mm

(c) 45° -dike with $H = 40$ mm

(d) 90° -dike with $H = 40$ mm

Figure 6 Normalized peak overpressure distributions on the ground for (a) a 45° -dike with $H = 20$ mm, (b) a 90° -dike with $H = 20$ mm, (c) a 45° -dike with $H = 40$ mm, and (d) 90° -dike with $H = 40$ mm.

reflection and diffraction at the dike. For the practical use of a 45° -dike, we should consider the directional characteristics of the weaker blast wave region around the line of $y = x$. The numerical results show that the blast wave strength is independent of height H for the 45° -dike. On the other hand, the 90° -dike has an intensification effect for the blast wave on the whole region of the ground and the dependency of height H for the blast wave strength on the ground. The higher 90° -dike gives a smaller mitigation region where the scaled distance is smaller than 10 m kg$^{-1/3}$ in Figure 6(b) and 5 m kg$^{-1/3}$ in Figure 6(d). In order to consider the explosives safety quantity-distance, we should discuss the height effect for the 90° -dike.

Dikes with different shapes result in different propagation behavior of the blast wave on the ground. Here, we use schematic pictures to discuss the effect of the reflection, diffraction, and three-dimensional structure of the dike, separately and qualitatively as shown in Figure 7. Blue, red, green and orange lines denote the blast wave, reflected wave, diffracted wave and the secondary shock wave by the dike, respectively. The brown point indicates the explosion point. Figures 7(a) and 7(b) show the reflection and diffraction of the blast wave at the 45° -dike and 90° -dike (side view), respectively. Left and right pictures in (b) denote the moments that the blast wave propagates on the dike and after it passes over the dike, respectively. Figure 7(c) shows the three-dimensional structure effect (top view) for the 45° -dike.

First, we discuss the diffraction effect at a dike. Diffraction by a dike weakens the strength of the blast wave. Therefore, the normalized peak overpressure near the dike becomes below 1 as shown in Figure 6. The angle of diffraction is defined as ϕ_{diff} of 90° for the 45° -dike and 135° for the 90° -dike as shown in Figures 7(a) and 7(b). As the larger post-shock flow divergence occurs with the 90° -dike, the effect of diffraction at the 90° -dike gives a large mitigation near the dikes as shown in Figure 5 in which

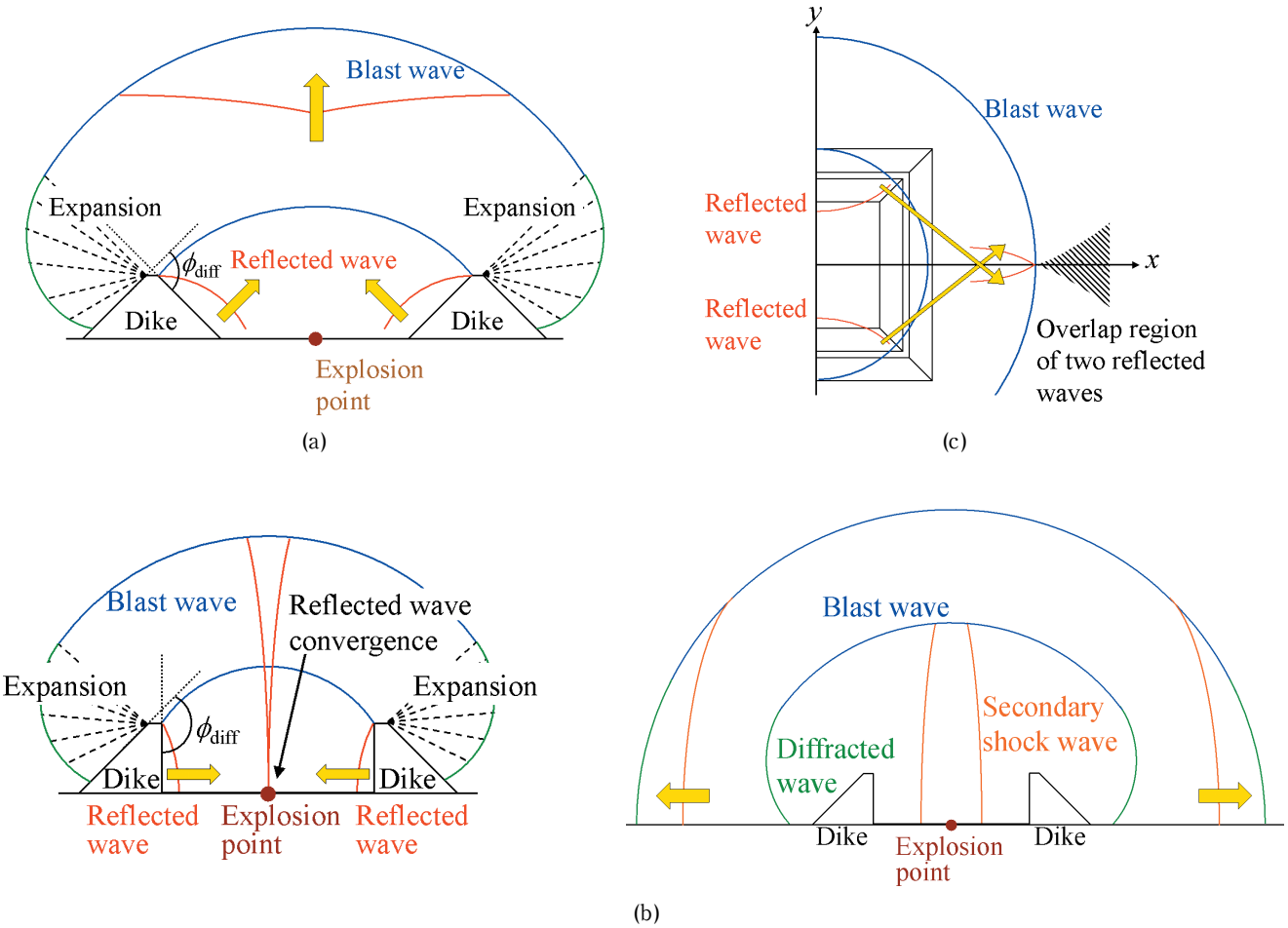

Figure 7 Schematic pictures of (a) reflection and diffraction of the blast wave at a 45°-dike (side view), (b) reflection and diffraction of the blast wave at a 90°-dike (side view), and (c) three-dimensional structure effect for a 45°-dike (top view). Blue, red, green, and orange lines denote the blast wave, reflected wave, diffracted wave, and the secondary shock wave by the dike, respectively. Left and right panels in (b) show the moments that the blast wave propagates on the dike and and after it passes over the dike, respectively.

minimum normalized peak overpressure after 45°- and 90°-dikes are 0.1 and 0.05, respectively.

Second, the reflection effect of the dike and the blast wave is discussed. Shock wave theory[15] gives that the shock wave propagating to the wedge shows self-similar flow patterns depending on the Mach number of the shock wave and the angle of the wedge. When the shock wave, whose Mach number is larger than 2, propagates on the 45°-wedge, the shock wave theory says that Mach reflection appears near the 45°-wedge. In the case of 45°-dike, as the blast wave reflects off the slope of the dike, Mach reflection appears. The reflected wave propagates upward, and a part of that affects the blast wave strength for the 45°-dike as shown in Figure 7(a). In this study, the initial condition of the blast wave, which starts to climb the slope, is independent of the height H, and the self-similar blast wave propagates on the slope. On the other hand, with the 90°-dike as shown in Figure 7(b), the reflected wave converges to the explosion point, and a secondary shock wave is generated at the explosion point. It follows, as shown in the right picture of Figure 7(b), and catches up with the blast wave, which intensifies the blast wave strength in the whole region on the ground. Around the line of $y = x$, stronger diffraction by adjoining two sides of the dike occurs, and the weakest diffracted wave appears. Then, the secondary shock wave at $y = x$ reaches the diffracted wave earlier than at other region. As height H increases, the reflected area of the blast wave enlarges. A weaker blast wave propagates after it passes over the dike, and a stronger secondary shock wave propagates from the explosion point. This shortens the distance in which the secondary shock wave reaches the blast wave, and the mitigation region of the blast wave strength becomes small as shown in Figures 6(b) and 6(d). This is the main factor that intensifies the blast wave strength on the ground for the 90°-dike.

Figure 7(c) shows the three-dimensional structure effect of the reflected wave for the 45°-dike. Reflected waves at the dike climb the adjoining side, and overlap at the scaled distance of 2-3 m kg$^{-1/3}$, as shown in the hatched region in which the blast wave strengthens. The hatched region makes the directional characteristics, but does not spread over all region on the ground, and the blast wave is always mitigated around $y = x$ as shown in Figures 6(a) and 6(c). As the reflected wave can easily climb the slope of the 45°-dike, the effect of the reflected wave is prominently visible. This is the main factor that intensifies the blast wave strength on the ground for the 45°-dike. The three-dimensional structure intensifies the blast wave strength on the ground.

This study implies that many factors having a complex structure need to be considered in order to discuss blast wave propagation. Using factors of the intensification and mitigation effect, we can propose a new dike. For example, the different size and angle of the dike result in weaker reflection and stronger diffraction, and an axisymmetric dike may reduce the blast wave strength (removal of the three-dimensional structure effect). Further study will propose a dike that minimizes blast wave strength.

5. Conclusion

The effect of a dike on a blast wave was investigated numerically and experimentally. The numerical results of the peak overpressure agree with the experimental results. The present study discussed the factors of the mitigation and intensification effects depending on the dike shape. A dike created complex flow features including the effects of reflection, diffraction, and three-dimensional structure. The complex interactions between them appear and determine mitigation and intensification of the blast wave. Further study will propose an optimal dike that minimizes blast wave strength.

Reference

1) S. Sudo, J. the Industrial Explosives Society (Sci. Tech. Energetic Materials), 23, 160 (1962) (in Japanese).
2) Y. Mizushima, J. the Industrial Explosives Society (Sci. Tech. Energetic Materials), 31, 361−377 (1970).
3) T. Homae, T. Matsumura, K. Wakabayashi, and Y. Nakayama, Sci. Tech. Energetic Materials, 69, 92−97 (2008).
4) T. Homae, T. Matsumura, K. Wakabayashi, and Y. Nakayama, Sci. Tech. Energetic Materials, 72, 155−160 (2011).
5) H. Miura, A. Matsuo, and G. Taguchi, J Loss Prev. Process Indust., 26, 329−337 (2013).
6) Y. Sugiyama, K. Wakabayashi, T. Matsumura, and Y. Nakayama, Science and Technology of Energetic Materials, accepted.
7) Y. Sugiyama, Y. Homae, K. Wakabayashi, T. Matsumura, and Y. Nakayama, Science and Technology of Energetic Materials, 75, 112−118 (2014).
8) Y. Sugiyama, Y. Homae, K. Wakabayashi, T. Matsumura, and Y. Nakayama, J Loss Prev. Process Indust., 32, 135−143 (2014).
9) G. Allaire, S. Clerc, and S. Kokh, J. Comput. Phys. 181, 577−616 (2002).
10) A. Harten, P.D. Lax, and B. van Leer, SIAM Review 25, 35−61 (1983).
11) E.F. Toro, M. Spruce, and W. Speares, Shock Waves 4, 25−34 (1994).
12) S.D. Kim, B.J. Lee, H.J. Lee, I.-S. Jeung, and J.-Y. Choi, Int. J. Numer. Meth. Fluids 62, 1107−1133 (2010).
13) X. Zhang and C.-W. Shu, Proc. R. Soc. A 467, 2752−2776 (2011).
14) C.-W. Shu and S. Osher, J. Comput. Phys. 77, 439−471 (1988).
15) J.D. Anderson, "Modern Compressible Flow With Historical Perspective", 3rd Ed., McGraw-Hill (2004).